Electronic Supplementary Material (ESI) for Journal of Materials Chemistry A.

Mass-Produced Metallic Multiwalled Carbon Nanotube Hybrids Exhibiting High N-type Thermoelectric Performances

Yizhuo Wang[1], Zhongxu Lu[3], Qiujun Hu[1], Xia Qi, Qing Li[1]*, Ziping Wu[3*], Hao-Li Zhang[4], Choongho Yu[5], Hong Wang[1,2,6]*

[1]Frontier Institute of Science and Technology, Xi'an Jiaotong University, Xi'an, 710054, China

[2]State Key Laboratory of Multiphase Flow in Power Engineering, Xi'an Jiaotong University, Xi'an, 710054, China

[3]School of Materials Science and Engineering, Jiangxi University of Science Technology, Ganzhou 341000, China

[4]State Key Laboratory of Applied Organic Chemistry (SKLAOC), College of Chemistry and Chemical Engineering, Lanzhou University, Lanzhou, 730000, China

[5]Mechanical Engineering Department, Texas A&M University, College Station, Texas 77843, USA

[6]ZhejiangYunFeng New Materials Technology Co., Ltd, No. 755 Hongji Street, Jindong District, Jinhua Zhejiang, 321015, China

E-mail: hong.wang@xjtu.edu.cn

EXPERIMENTAL SECTION

Materials

Triphenylphosphine (TPP) (99 %) was purchased from ALADDIN, U.S.A. Polyethyleneimine (PEI) (99 %) was purchased from MACKLIN Co., Ltd., China.

Diethylenetriamine (DETA) (99 %) was purchased from ENERGY CHEMICAL Co., Ltd., China. 1,3-Dimethyl-2-phenyl-2,3-dihydro-1H-benzoimidazole (N-DMBI) (98 %) was purchased from Sigma-Aldrich Co., Ltd., U.S.A. 2,3,5,6-Tetrafluoro-7,7,8,8-tetracyanoquinodimethane (F4TCNQ) (97%) was purchased from MACKLIN Co., Ltd.,China. 7,7,8,8-Tetracyanoquinodimethane (TCNQ) (98%) was purchased from J&K Chemicals Co., Ltd.,China. All the other used chemicals in the work were of reagent grade and were used without any further purification.

Synthesis of MWCNT:

Pristine MWCNT mats were synthesized by a methanol-mediated chemical vapor deposition (CVD) method at ~1150 ^{o}C.[1-4] Briefly, the CVD was performed with a horizontal furnace. Methanol and n-hexane with the ratio of 1:9 were used as a carbon source, ferrocene was used as a catalyst precursor (20 mg/cm^3 and thiophene as a growth promoter (3 µl/cm^3). Nitrogen was used as the carrier gas at a flow rate of 1000 ml/min. The reactor was a quartz tube with an inner diameter of 100 mm. Aluminum foil with a thickness of 0.5 mm was used as the substrate. The foil was pre-cleaned with ethanol and 10% HCl in advance.

Synthesis of graphene oxide (GO):

GO was synthesized from graphite flakes (Sigma-Aldrich, USA) with an improved method reported by Tour et. al.[5] Briefly, graphite flakes (3.0 g) were added into a 9:1 mixture of concentrated H_2SO_4/H_3PO_4 (360:40 mL). After stirred for 60 min, the obtained solution was transferred to an ice bath and the temperature was cooled down to 0 ^{o}C. $KMnO_4$ (6 wt.% equiv) was added slowly into the solution at 0 ^{o}C. Then, the solution was warmed up to 50 ^{o}C and stirred

for 24 h. After that, the solution was cooled down to 0 ^{o}C again with an ice bath. 30% H_2O_2 (3 mL) was added dropwise. The solution was then stirred for 20 min before centrifuged (5000 rpm, 10 min). The obtained solid was washed thoroughly with water until the PH value of the supernate is ~7. At last, the obtained solid was dried in a vacuum.

Preparation of MWCNT/GO hybrids:

8 mg homemade GO was dispersed in a mixed solution (200 ml) with DI water and alcohol at the ratio of 1:1. After sonicated with a bath sonicator for 10 min at room temperature, the obtained solution was spread on the MWCNT film with an estimated ratio of 0.4-0.5 mg per centimeter square of MWCNT film with the weight ratio of 1:3 for GO: MWCNT.

The synthesis process has been illustrated in Figure S1 in the supporting information. The conveyor belt was covered by an aluminum foil as a substrate. Carbon nanotubes were generated continuously from the furnace, which fell on the conveyor belt to form a film. Then, GO solution was sprayed on the film. After the conveyor belt ran one circle, an MWCNT/GO bilayer was obtained. 2 bilayers, 4 bilayers, and 8 bilayers were obtained when the conveyor belt ran 2 circles, 4 circles, and 8 circles, respectively. When the synthesis process is completed, the thin film could be peeled off from the substrate.

Preparation of n-type and p-type dopant solutions: The n-type and p-type dopants were dissolved in dimethylsulfoxide (DMSO) at certain concentrations by weight.

Preparation of n-type and p-type MWCNT/GO hybrids : The pristine MWCNT/GO hybrids was cut into strips with a length of ~25 mm in length and width of ~5 mm. Then the MWCNT/GO strip was soaked in the prepared solutions of n-type (p-type) dopants for 2 hours. After that, it was washed with DI water thoroughly and dried in a vacuum oven at 60 ^{o}C.

Device fabrication: The TE performance of a flexible device made of MWCNT/GO-NDMBI (n-type module) and MWCNT/GO-F4TCNQ (p-type module) was measured. The device is composed of 5 n-type legs and 5 p-type

legs, which are alternatively connected in series with conductive copper tape as shown in Figure 5b. Each leg has a width of ~ 5 mm and a length of ~25 mm.

Measurements: The conductivity and Seebeck coefficient were measured with SBA-458, NETZSCH, Germany. The output voltage and output power of TE modules were measured using a Keithley 2400 Multimeter (Keithley Instruments Inc., USA). Raman spectra were recorded within the wavenumber range of 800−3500 cm^{-1} through a Raman spectrometer (Laser Raman Spectrometer) with an excitation wavelength of 514 nm. Scanning electron microscope images were obtained with a field-emission scanning electric microscopy (FEI Sirion 200) and tunneling electron microscope images were obtained with JEOL 2010F, accelerating voltage, 200 kV. Thermogravimetric analyses (TGA) of the MWCNT mats were measured under the nitrogen atmosphere by Synchronous Thermal Analyzer Q600 at a heating rate of 10 °C min^{-1}. X-ray photoelectron spectroscopy and ultraviolet photoelectron spectroscopy were performed with Thermo Fisher ESCALAB Xi+ to determine the work function of MWCNT mats. Mechanical properties were measured using Netzsch DMA242E. Hall effect measurement was performed with LakeShore 8404.

The details of theoretical calculation on the thermoelectric properties of MWCNT and MWCNT/GO: The theoretical calculation has been performed to qualitatively understand the high TE performance of NDMBI-doped MWCNT/GO samples. Metallic MWCNT (6, 6)@(11, 11)@(16, 16) and semiconducting MWCNT MWCNT (11, 0)@(20, 0)@(29, 0) were used in the calculation. In general, CNTs have different rolling structures which are typically described by (n,m) chiral indices. When 2n+m=3q (q is an integer), the CNT behaves like a metal. Otherwise, it is a semiconductor.[6] MWCNT can be regarded as consisting of multiple layers of carbon nanotubes. Three-layer structure MWCNTs were used in the calculation. For metallic MWCNT, (6, 6) is a metallic CNT with a small diameter which represents the inner layer of the

metallic MWCNT. (11, 11) and (16, 16) represent the middle layer and the outer layer of the MWCNT, respectively. For semiconducting MWCNTs, (11, 0), (20, 0), and (29, 0) were used as the inner, the middle, and the outer layer of the MWCNTs. It is a widely used method to describe the layers and rolling structures with (n, m)@(n, m)@(n, m).[7]

According to Landauer formula, the Seebeck coefficient S(μ) and conductance G(μ) to the chemical potential μ can be described as follows:

$$S(\mu) = \frac{1}{qT}\frac{\int dET(E)(-\frac{\partial f(E,\mu)}{\partial E})(E-\mu)}{\int dET(E)(-\frac{\partial f(E,\mu)}{\partial E})} \quad (1)$$

$$G(\mu) = \frac{2q^2}{h}\int dET(E)(-\frac{\partial f(E,\mu)}{\partial E}) \quad (2)$$

where *q*, *h*, *f(E, μ),* and *T(E)* are the charge of carriers, the Planck constant, the Fermi-Dirac distribution function, and the transmission function, respectively. The theoretical calculation was implemented in the ATK package (Ver. 2013.8.0). There were three regions: a device region, a left electrode, and a right electrode. The device region has a length of 10 unit cells for both metallic and semiconducting MWCNTs. The thermoelectric properties of metallic MWCNT (6, 6)@(11, 11)@(16, 16) and semiconducting MWCNT (11, 0)@(20, 0)@(29, 0) was calculated by using the tight-binding method with 1x1x100 Monkhorst-Pack K-grid. The used Slater-Koster parameters were obtained by the density-functional tight-binding method with the “hotbit” code.[8] T(E) of MWCNTs was calculated by combing the nonequilibrium Green’s function method with the tight-binding method.

The band structure of (6, 6)@(11, 11)@(16, 16)-GO before and after Fe and N-DMBI doping were calculated by ATK package (Ver. 2013.8.0). The geometry was optimized with ATK-SE and the band structure was obtained by density functional theory (DFT) with the exchange-correlation functional of GGA-PBE.

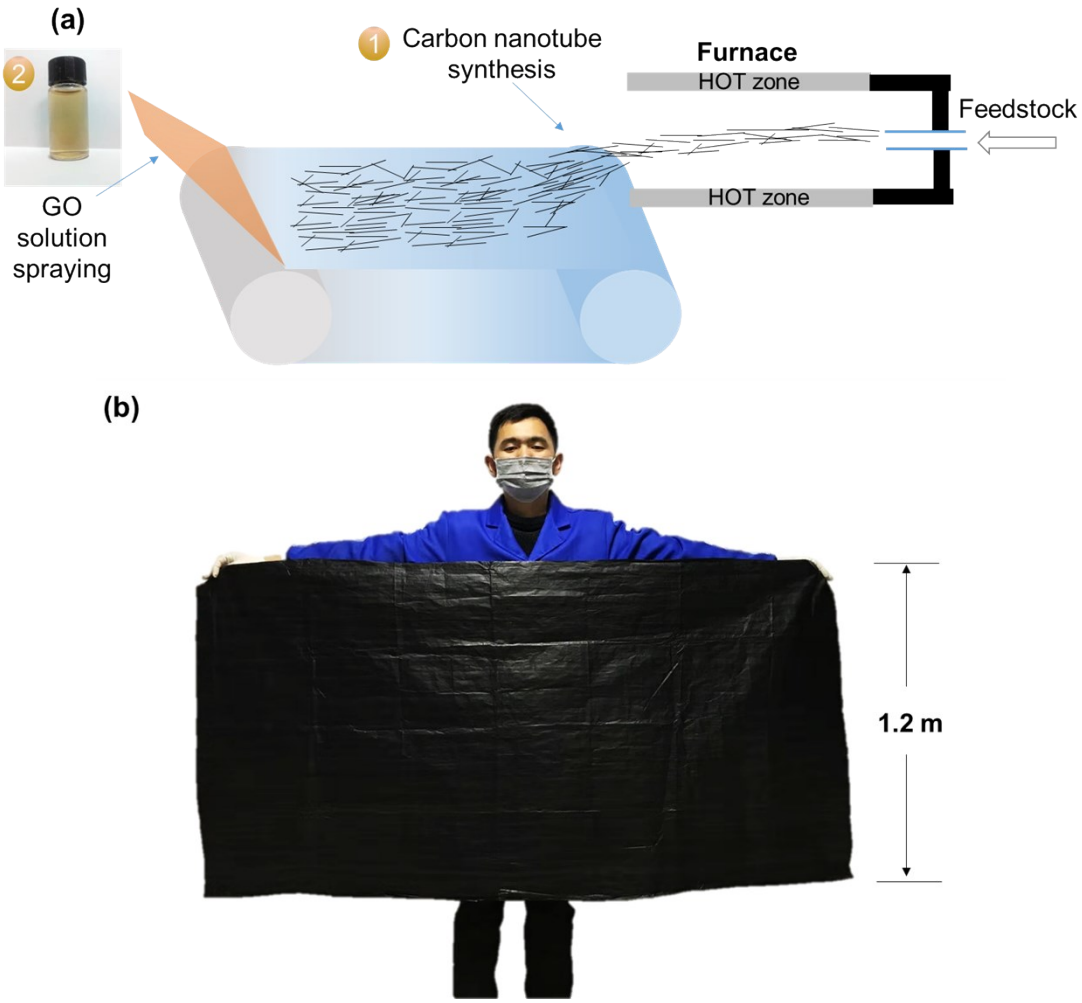

Figure S1 (a) Illustration of the synthesis process of the layer-by-layer MWCNT/GO hybrid. (b) Photograph of an MWCNT/GO hybrid film with a width of ~1.2 m and a length of ~2.3 m.

Table S1 Thermoelectric properties of pristine MWCNT/GO samples with different bilayers.

Pristine MWCNT/GO Samples		**σ（S/cm）**	**S（μV/K）**	**PF（μW/m K^2）**
2 Bilayers	Sample 1	385	53	109
	Sample 2	416	53	120
	Sample 3	456	54	136
	Average	419±29.1	54±0.6	122±11.2
4 Bilayers	Sample 1	397	54	115
	Sample 2	385	55	117
	Sample 3	468.76	51	123
	Average	417±36.9	53±1.6	118±3.4
8 Bilayers	Sample 1	434	53	123
	Sample 2	384	54	111
	Sample 3	406	55	103
	Average	408±20.7	53.95±0.7	119±5.6

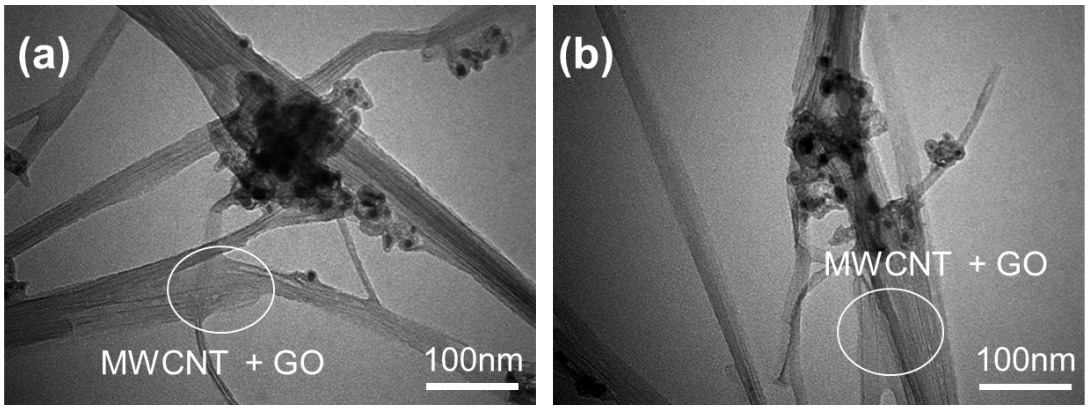

Figure S2 Transmission electron microscope (TEM) images of pristine MWCNT/GO (a) and MWCNT/GO-NDMBI$_{7wt}$ (b).

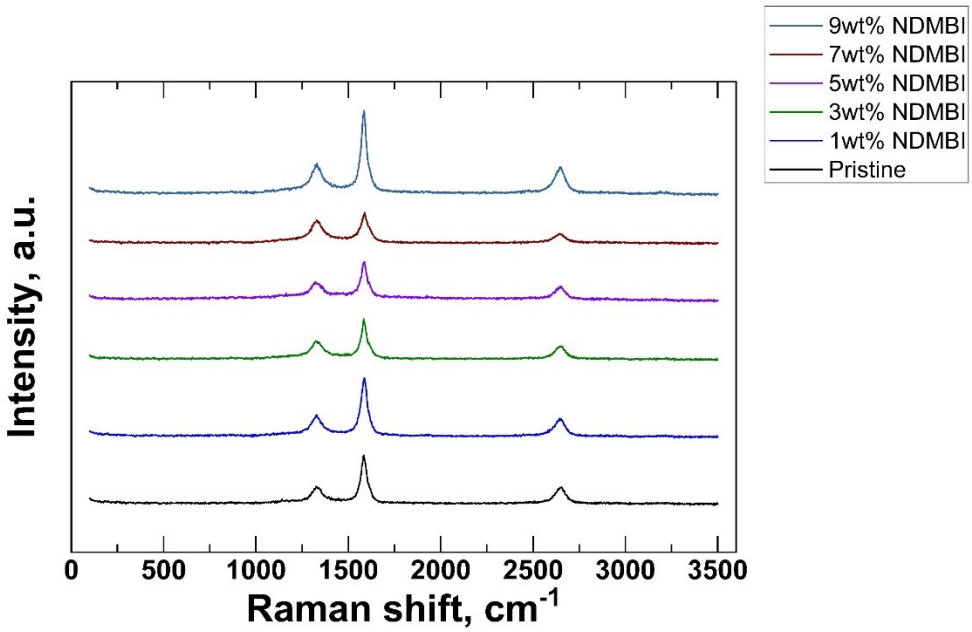

Figure S3 Raman spectra for MWCNT/GO doped by N-DMBI at different concentrations.

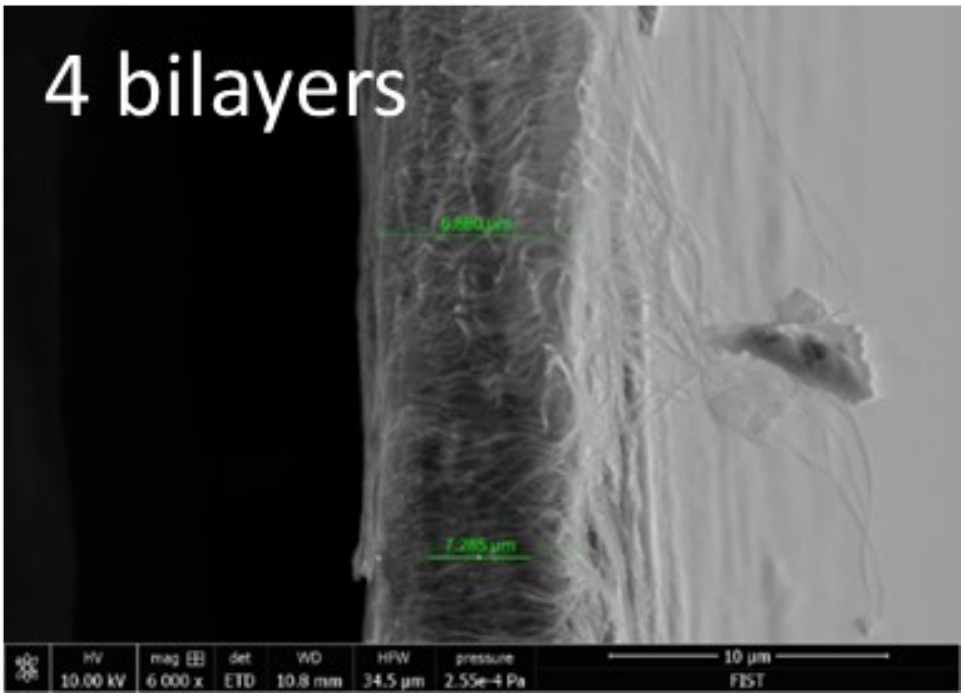

Figure S4 SEM image of the cross-section of the MWCNT/GO with 4 bilayers.

Table S2 Hall measurement results for pristine MWCNT/GO before and after p-/n- type dopant treatment.

	Carrier mobility, $cm^2/V\text{-}s$	Carrier concentration, cm^{-3}
Pristine MWCNT/GO	0.56	5.2×10^{21}
MWCNT/GO-TCNQ	0.82	3.9×10^{21}
MWCNT/GO-F4TCNQ	1.05	4.6×10^{21}
MWCNT/GO-$NDMBI_{5wt}$	0.68	7.3×10^{21}
MWCNT/GO-$NDMBI_{7wt}$	0.81	8.8×10^{21}
MWCNT/GO-DETA	0.40	5.2×10^{21}
MWCNT/GO-PEI	0.15	17.6×10^{21}
MWCNT/GO-TPP	0.26	8.9×10^{21}

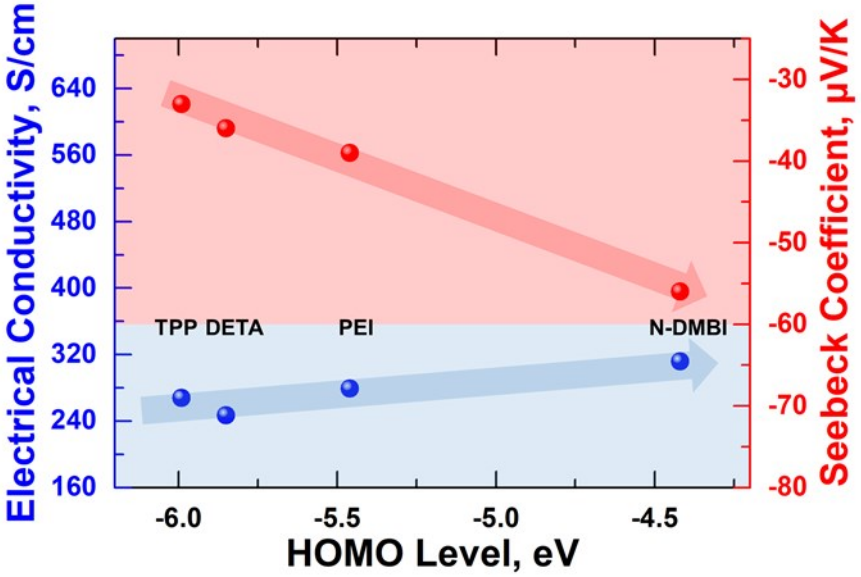

Figure S5 Electrical conductivity and Seebeck coefficient of MWCNT doped with different n-type dopants.

Table S3 Comparison of the properties of CNT-based flexible thermoelectric materials.

Material	Electrical conductivity (S/cm)	Seebeck coefficient (μV/K)	Power factor $\mu W/m^{-1}K^{-2}$	Reference
a-CNT web/BV	2228	−116	3103	[9]
SWCNT/PEI	3630	−64	1500	[10]
TDAE–PEDOT/CNT	7.3	−1200	1050	[11]
MWCNT/PEI	2003	-51	521	[12]
DWNT–PEI/rGO	460	-93	400	[13]
CNT/KOH/18-crown-6-ether	2050	−33	230	[14]
MWCNT-Graphene/N-DMBI	920	-46	195	This work
DWCNT–PEI/graphene–PVP	300	−80	190	[15]
SWCNT/CTAB	840	−47	185.7	[16]
SWCNT/TPM-CB	497	−59	172	[17]
SWCNT/NDINE	400	−57	135	[18]
SWCNT/PDINE	500	−47.5	112	[18]
$CoCp_2$ @SWCNT	432	−41.8	75.4	[19]
CNTs/PEI/DETA-$NaBH_4$	52	−86	38	[20]
CNTs/PEI–$NaBH_4$	60	−77	35.6	[21]
SWCNT/DETA–CaH_2	165	−41	27.7	[22]
SWCNT/dppp	100	−52	27	[23]
SWCNT/tpp	48	−72	25	[23]
CPE–$PyrBIm_4$ /SWCNT	106	−41	17.8	[24]
CNTs/PEI/DETA	39	−63	15.5	[20]
CNTs/PEI	30	–57	9.7	[21]
MWCNT polyvinylpyrrolidone	77	-16	1.98	[25]
As growth MWCNT	110	-5	0.275	[26]
MWCNT Yarn +PVP	1	-14	0.02	[27]
rGO Thermal Annealing Temperature	-	-11.3	-	[28]

Table S4 Power output of a fabricated device measured three times at each temperature gradient.

△T (K)		Output power (nW)	Output power per unit weight (μW/g)	Output power per unit area (W/m^2)
10	1	29.676	5.935	0.106
	2	30.244	6.049	0.108
	3	30.962	6.192	0.111
	Average	30.29±0.53	6.06±0.11	0.11±0.01
20	1	111.471	22.294	0.398
	2	113.672	22.734	0.406
	3	112.294	22.459	0.401
	Average	112.48±0.91	22.50±0.18	0.40±0.01
30	1	293.574	58.715	1.048
	2	297.140	59.428	1.061
	3	299.38	59.876	1.069
	Average	296.70±2.39	59.34±0.48	1.06±0.01
40	1	498.280	99.656	1.780
	2	501.179	100.236	1.790
	3	495.966	99.193	1.771
	Average	498.48±2.13	99.70±0.43	1.78±0.01
50	1	786.363	157.273	2.808
	2	791.463	158.293	2.827
	3	795.848	159.170	2.842
	Average	791.22±3.88	158.24±0.78	0.83±0.01
60	1	1216.450	243.290	4.345
	2	1209.219	241.844	4.319
	3	1211.927	242.385	4.328
	Average	1212.53±2.98	242.51±0.06	4.33±0.01

$\Delta T = T_{hot} - T_{cold}$, where ΔT, T_{hot}, T_{cold} are the temperature gradient, the temperature of the hot side, and the temperature of the cold side (room temperature 25 ^{o}C). The error (E) was calculated according to the following relation:

$$E = [\sum_{i=1}^{n} (X_i - X_m)^2 / n]^{0.5} \quad \text{and} \quad X_m = \sum_{i=1}^{n} X_i / n$$

Where X_i and n are experimental data and the number of samples, respectively.

Table S5 Comparison of output power per area of CNT based flexible thermoelectric devices.

Material	Number of p-n pair	Output power per area(W/m^2)	△T(K)	Reference
CNT foam	8	0.004	13.9	[29]
CNT yarn	966	0.0515	47.5	[30]
SWCNT web	10	0.02	20	[10]
SWCNT	3	1.67	27.5	[10]
MWCNT/graphene	5	4.30	60	This work

1st time testing

2nd time testing

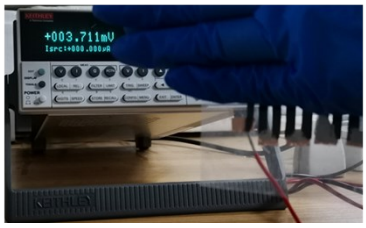

3rd time testing

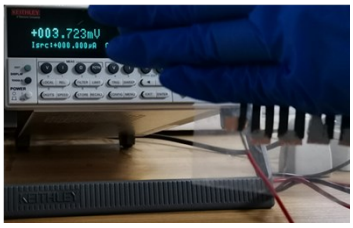

Figure S6 Output voltage testing of the original fabricated device three times after over 170 days.

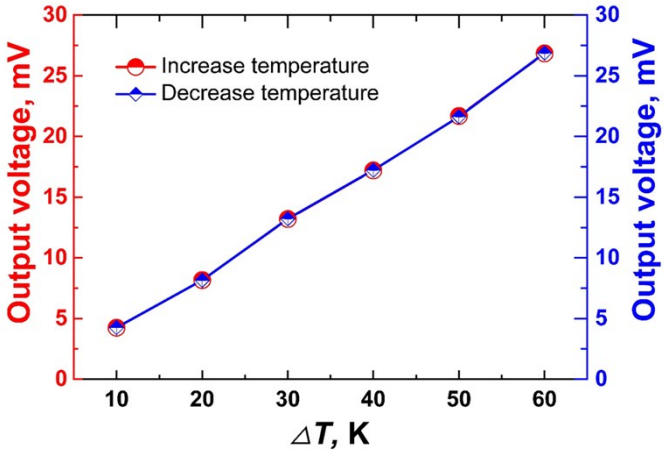

Figure S7 Output voltage testing of the newly fabricated device in the temperature range of 298 K to 358 K.

Table S6 Seebeck coefficients and power factors of previously reported MWCNT based n-type TE materials

Material	**Seebeck Coefficient(μV/K)**	**Power Factor(μW/m^{-1}K^{-2})**	**Reference**
MWCNT/PVP	-14	0.020	[27]
PVP/MWCNT/PEI	-23.5	1.98	[25]
$CuSbSe_2$ /MWCNT/PANI	-23.5	1.16	[31]
$CuInSe_2$ /MWCNT/PANI	-6.1	0.14	[31]
$AgInSe_2$ /MWCNT/PANI	-4.1	0.03	[31]
MWCNT/PEI	-6	0.06	[32]
Photoinduced P3HT/MWCNT	-10	0.01	[33]
CuSe NPs/MWCNT/PANI	-28	3.6	[31]
In_2Se_3 NPs/MWCNT/PANI	-24	1.75	[31]
Sb_2Se_3 NPs/MWCNT/PANI	-10	0.49	[31]

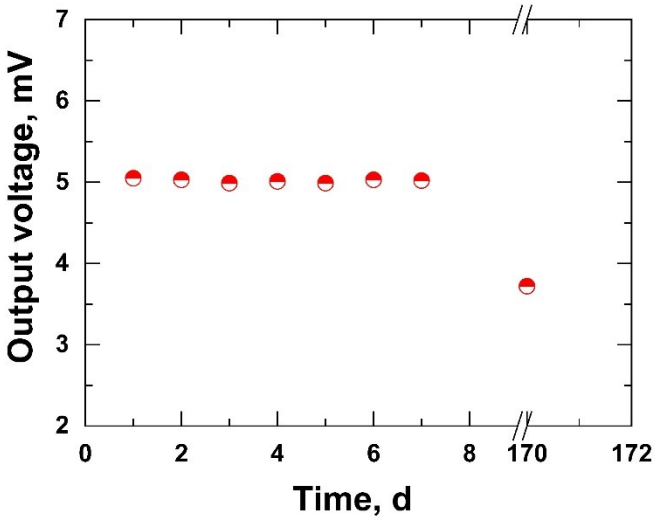

Figure S8 Output voltage testing device at room temperature in the air.

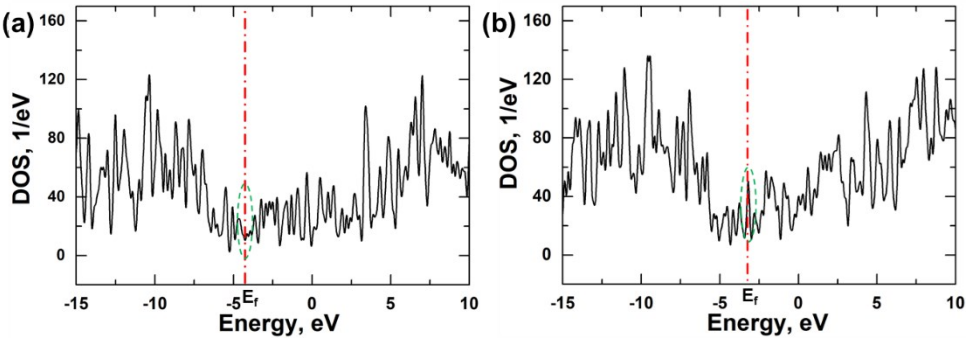

Figure S9 the calculated DOS of MWCNT/GO, and NDMBI-doped MWCNT/GO. Metallic MWCNT (6, 6)@(11, 11)@(16, 16) was used.

Figure S9 shows the DOS of MWCNT/GO before (a) and after (b) doping. It is clear that the DOS near Fermi level for Fe and N-DMBI doped MWCNT/GO increases, which subsequently leads to an increase of the Seebeck coefficient.

References

1. J. W. Hu, Z. P. Wu, S. W. Zhong, W. B. Zhang, S. Suresh, A. Mehta and N. Koratkar, *Carbon*, 2015, **87**, 292-298.
2. Z. Wu, K. Liu, C. Lv, S. Zhong, Q. Wang, T. Liu, X. Liu, Y. Yin, Y. Hu, D. Wei and Z. Liu, *Small*, 2018, **14**, e1800414.
3. B. J. Han, T. Liu, Z. J. Huang, D. M. Chen, Y. S. Zhu, C. Y. Zhou, Y. S. Li, Y. H. Yin and Z. P. Wu, *Appl. Phys. Lett.*, 2017, **110**, 103902.
4. Z. P. Wu, D. M. Cheng, W. J. Ma, J. W. Hu, Y. H. Yin, Y. Y. Hu, Y. S. Li, J. G. Yang and Q. F. Xu, *AIP Adv.*, 2015, **5**, 067130.
5. D. C. Marcano, D. V. Kosynkin, J. M. Berlin, A. Sinitskii, Z. Sun, A. Slesarev, L. B. Alemany, W. Lu and J. M. Tour, *ACS Nano*, 2010, **4**, 4806-4814.
6. N. Hamada, S.-i. Sawada and A. Oshiyama, *Phys. Rev. Lett.*, 1992, **68**, 1579-1581.
7. W. S. Su, T. C. Leung and C. T. Chan, *Phys. Rev. B*, 2007, **76**, 235413.
8. P. Koskinen and V. Mäkinen, *Comput. Mater. Sci.*, 2009, **47**, 237-253.
9. C. J. An, Y. H. Kang, H. Song, Y. Jeong and S. Y. Cho, *J. Mater. Chem. A*, 2017, **5**, 15631-15639.
10. W. Zhou, Q. Fan, Q. Zhang, L. Cai, K. Li, X. Gu, F. Yang, N. Zhang, Y. Wang, H. Liu, W. Zhou and S. Xie, *Nat. Commun.*, 2017, **8**, 14886.
11. H. Wang, J.-H. Hsu, S.-I. Yi, S. L. Kim, K. Choi, G. Yang and C. Yu, *Adv. Mater.*, 2015, **27**, 6855-6861.
12. K. Chatterjee, A. Negi, K. Kim, J. Liu and T. K. Ghosh, *ACS Appl. Energy Mater.*, 2020, **3**, 6929-6936.
13. J.-H. Hsu and C. Yu, *Nano Energy*, 2019, DOI: https://doi.org/10.1016/j.nanoen.2019.104282, 104282.
14. Y. Nonoguchi, M. Nakano, T. Murayama, H. Hagino, S. Hama, K. Miyazaki, R. Matsubara, M. Nakamura and T. Kawai, *Adv. Funct. Mater.*, 2016, **26**, 3021-3028.
15. H. Wang, J.-H. Hsu, G. Yang and C. Yu, *Adv. Mater.*, 2016, **28**, 9545-9549.
16. X. Cheng, X. Wang and G. Chen, *J. Mater. Chem. A*, 2018, **6**, 19030-19037.
17. Y. Nonoguchi, A. Tani, T. Ikeda, C. Goto, N. Tanifuji, R. M. Uda and T. Kawai, *Small*, 2017, **13**, 1603420.
18. G. Wu, Z.-G. Zhang, Y. Li, C. Gao, X. Wang and G. Chen, *ACS Nano*, 2017, **11**, 5746-5752.
19. L. J. Li, A. N. Khlobystov, J. G. Wiltshire, G. A. D. Briggs and R. J. Nicholas, *Nat. Mater.*, 2005, **4**, 481-485.
20. S. L. Kim, K. Choi, A. Tazebay and C. Yu, *ACS Nano*, 2014, **8**, 2377-2386.
21. C. Yu, A. Murali, K. Choi and Y. Ryu, *Energy Environ. Sci.*, 2012, **5**, 9481-9486.
22. G. Wu, C. Gao, G. Chen, X. Wang and H. Wang, *J. Mater. Chem. A*, 2016, **4**, 14187-14193.
23. Y. Nonoguchi, K. Ohashi, R. Kanazawa, K. Ashiba, K. Hata, T. Nakagawa, C. Adachi, T. Tanase and T. Kawai, *Sci. Rep.*, 2013, **3**, 3344-3344.
24. C.-K. Mai, B. Russ, S. L. Fronk, N. Hu, M. B. Chan-Park, J. J. Urban, R. A. Segalman, M. L. Chabinyc and G. C. Bazan, *Energy Environ. Sci.*, 2015, **8**, 2341-2346.

25. R. Sarabia-Riquelme, J. Craddock, E. A. Morris, D. Eaton, R. Andrews, J. Anthony and M. C. Weisenberger, *Synth. Met.*, 2017, **225**, 86-92.
26. B. Kumanek, G. Stando, P. S. Wrobel and D. Janas, *Materials (Basel, Switzerland)*, 2019, **12**, 3567.
27. J. D. Ryan, A. Lund, A. I. Hofmann, R. Kroon, R. Sarabia-Riquelme, M. C. Weisenberger and C. Müller, *ACS Appl. Energy Mater.*, 2018, **1**, 2934-2941.
28. N. D. K. Tu, J. Choi, C. R. Park and H. Kim, *Chem. Mat.*, 2015, **27**, 7362-7369.
29. M.-H. Lee, Y. H. Kang, J. Kim, Y. K. Lee and S. Y. Cho, *Adv. Energy Mater.*, 2019, **9**, 1900914.
30. Y. Zheng, Q. Zhang, W. Jin, Y. Jing, X. Chen, X. Han, Q. Bao, Y. Liu, X. Wang, S. Wang, Y. Qiu, C.-a. Di and K. Zhang, *J. Mater. Chem. A*, 2020, **8**, 2984-2994.
31. A. S. Kshirsagar, C. Hiragond, A. Dey, P. V. More and P. K. Khanna, *ACS Appl. Energy Mater.*, 2019, **2**, 2680-2691.
32. M. Bharti, A. Singh, B. P. Singh, S. R. Dhakate, G. Saini, S. Bhattacharya, A. K. Debnath, K. P. Muthe and D. K. Aswal, *J. Power Sources*, 2020, **449**, 227493.
33. B. Dörling, J. D. Ryan, J. D. Craddock, A. Sorrentino, A. E. Basaty, A. Gomez, M. Garriga, E. Pereiro, J. E. Anthony, M. C. Weisenberger, A. R. Goñi, C. Müller and M. Campoy-Quiles, *Adv. Mater.*, 2016, **28**, 2782-2789.